Chemical Geology 260 (2009) 286–300

Contents lists available at ScienceDirect

Chemical Geology

journal homepage: www.elsevier.com/locate/chemgeo

The hydromagnesite playas of Atlin, British Columbia, Canada: A biogeochemical model for CO_2 sequestration

Ian M. Power [a,*], Sasha Wilson [b], James M. Thom [b], Gregory M. Dipple [b,c], Janet E. Gabites [c], Gordon Southam [a]

[a] Department of Earth Sciences, The University of Western Ontario, London, Ontario, Canada N6A 5B7
[b] Mineral Deposit Research Unit, Department of Earth and Ocean Sciences, The University of British Columbia, Vancouver, British Columbia, Canada V6T 1Z4
[c] Pacific Centre for Isotopic and Geochemical Research, Department of Earth and Ocean Sciences, The University of British Columbia, Vancouver, British Columbia, Canada V6T 1Z4

ARTICLE INFO

Article history:
Received 6 October 2008
Received in revised form 5 January 2009
Accepted 9 January 2009

Editor: J. Fein

Keywords:
Carbon dioxide sequestration
Mineral carbonation
Bacteria
Magnesite
Hydromagnesite

ABSTRACT

Anthropogenic greenhouse gas emissions may be offset by sequestering carbon dioxide (CO_2) through the carbonation of magnesium silicate minerals to form magnesium carbonate minerals. The hydromagnesite [$Mg_5(CO_3)_4(OH)_2 \cdot 4H_2O$] playas of Atlin, British Columbia, Canada provide a natural model to examine mineral carbonation on a watershed scale. At near surface conditions, CO_2 is biogeochemically sequestered by microorganisms that are involved in weathering of bedrock and precipitation of carbonate minerals. The purpose of this study was to characterize the weathering regime in a groundwater recharge zone and the depositional environments in the playas in the context of a biogeochemical model for CO_2 sequestration with emphasis on microbial processes that accelerate mineral carbonation.

Regions with ultramafic bedrock, such as Atlin, represent the best potential sources of feedstocks for mineral carbonation. Elemental compositions of a soil profile show significant depletion of MgO and enrichment of SiO_2 in comparison to underlying ultramafic parent material. Polished serpentinite cubes were placed in the organic horizon of a coniferous forest soil in a groundwater recharge zone for three years. Upon retrieval, the cube surfaces, as seen using scanning electron microscopy, had been colonized by bacteria that were associated with surface pitting. Degradation of organic matter in the soil produced chelating agents and acids that contributed to the chemical weathering of the serpentinite and would be expected to have a similar effect on the magnesium-rich bedrock at Atlin. Stable carbon isotopes of groundwater from a well, situated near a wetland in the southeastern playa, indicate that ~12% of the dissolved inorganic carbon has a modern origin from soil CO_2. The mineralogy and isotope geochemistry of the hydromagnesite playas suggest that there are three distinct depositional environments: (1) the wetland, characterized by biologically-aided precipitation of carbonate minerals from waters concentrated by evaporation, (2) isolated wetland sections that lead to the formation of consolidated aragonite sediments, and (3) the emerged grassland environment where evaporation produces mounds of hydromagnesite. Examination of sediments within the southeastern playa–wetland suggests that cyanobacteria, sulphate reducing bacteria, and diatoms aid in producing favourable geochemical conditions for precipitation of carbonate minerals.

The Atlin site, as a biogeochemical model, has implications for creating carbon sinks that utilize passive microbial, geochemical and physical processes that aid in mineral carbonation of magnesium silicates. These processes could be exploited for the purposes of CO_2 sequestration by creating conditions similar to those of the Atlin site in environments, artificial or natural, where the precipitation of magnesium carbonates would be suitable. Given the vast quantities of Mg-rich bedrock that exist throughout the world, this study has significant implications for reducing atmospheric CO_2 concentrations and combating global climate change.

1. Introduction

Atmospheric concentrations of greenhouse gases (e.g., carbon dioxide, methane, and nitrous oxide) have increased significantly as a result of human activities since the pre-industrial era (AD 1000–1750). Most notably, carbon dioxide (CO_2) has increased from a pre-industrial level of approximately 275–285 ppm to 379 ppm in 2005, which has been caused mainly by fossil fuel consumption and to a lesser extent land use changes (Solomon et al., 2007). The increase in globally averaged temperatures since the mid-20th century can very likely be attributed to the increase in anthropogenic greenhouse gases (Metz et al., 2005). One means of reducing net greenhouse gas emissions is through the capture and storage of CO_2. Several methods

* Corresponding author. Tel.: +1 519 661 3187; fax: +1 519 661 3198.
E-mail addresses: ipower@uwo.ca (I.M. Power), swilson@eos.ubc.ca (S. Wilson), jthom@eos.ubc.ca (J.M. Thom), gdipple@eos.ubc.ca (G.M. Dipple), jgabites@eos.ubc.ca (J.E. Gabites), gsoutham@uwo.ca (G. Southam).

0009-2541/$ – see front matter © 2009 Elsevier B.V. All rights reserved.
doi:10.1016/j.chemgeo.2009.01.012

have been proposed including mineral carbonation, oceanic storage, underground injection for enhanced fossil fuel recovery, and injection into saline aquifers (Giammar et al., 2005; Metz et al., 2005; Xu et al., 2005).

Mineral carbonation has traditionally been defined as a chemical process that involves the reaction of CO_2 with silicate minerals to form carbonate minerals (Lackner et al., 1995; Gerdemann et al., 2007). However, this reaction is a natural process of weathering that has occurred over geological time and currently sequesters an estimated 100 million tons of carbon each year (Siefritz, 1990). The abundance of silicate minerals and the formation of a stable form of carbon, as carbonate minerals, are advantageous in that carbon storage is easily verifiable and stable on a geologic timescale. Ultramafic rocks typically contain high proportions of magnesium oxide (up to 50% by weight) in comparison to the CaO in calcium silicate rocks. For this reason, ophiolite belts that contain high abundances of magnesia as serpentine and olivine represent the best potential feedstock for mineral carbonation (Metz et al., 2005). The chemical reactions for the direct carbonation of serpentine and olivine are given in Eqs. (1) and (2) (Lackner et al., 1995; Metz et al., 2005).

$$Mg_2SiO_4 + 2CO_2 \rightarrow 2MgCO_3 + SiO_2 \quad (1)$$

$$Mg_3Si_2O_5(OH)_4 + 3CO_2 \rightarrow 3MgCO_3 + 2SiO_2 + 2H_2O \quad (2)$$

In the Atlin, British Columbia region, Hansen et al. (2005) documented the controls on the formation of listwanite, a carbonate altered serpentinite, in the ultramafic rocks of Monarch Mountain. The hydrothermal transformation of these rocks is similar to industrial processes that are being considered for CO_2 sequestration using mineral carbonation. Lackner et al. (1995) used chemical treatment with high temperature and pressure to accelerate ex situ mineral carbonation, which they proposed could be implemented on an industrial scale. However, the current state of this technology requires a large input of energy and is more expensive than most other applications of geological storage (Metz et al., 2005). For these reasons, CO_2 sequestration by this means may not be feasible on a large scale. Alternatively, Kelemen and Matter (2008) have proposed in situ carbonation of peridotite and have shown that 10^4 to 10^5 tons per year of CO_2 is sequestered by natural carbonation of the Samail ophiolite, Sultanate of Oman.

In contrast to chemical treatment, biological processes involved in natural mineral carbonation have been largely unexplored. Ferris et al. (1994) suggested that weathering of silicate minerals in bedrock is biogeochemically coupled to the precipitation of carbonate minerals by microorganisms. The soil biota enhance weathering rates by increasing the partial pressure of CO_2, generating chelating agents, and both inorganic and organic acids (Schwartzman and Volk, 1989; Oh and Richter, 2004). Microbial processes that mediate or promote carbonate precipitation include photosynthesis, ammonification, denitrification, sulphate reduction, anaerobic sulphide oxidation, methanogenesis, and manganese and iron oxide reduction (Ferris et al., 1994; Riding, 2000; Roberts et al., 2004). With particular relevance to this study, biologically-aided precipitation of dypingite $[Mg_5(CO_3)_4(OH)_2 \cdot 5H_2O]$ was experimentally demonstrated by Power et al. (2007) using cyanobacteria cultured from the Atlin site. The combined processes of bedrock weathering and carbonate precipitation by oxygenic phototrophic microorganisms are described by Eq. (3) (Ferris et al., 1994).

$$(Ca,Mg)SiO_3 + 2H_2CO_3 + H_2O \rightarrow (Ca,Mg)CO_3 + CH_2O + H_4SiO_4 + O_2 \quad (3)$$

The hydromagnesite playas near Atlin provide a natural model for developing a passive process for CO_2 sequestration that involves (1) the weathering of ultramafic rock and (2) precipitation of magnesium carbonate minerals via a pathway that is mediated by microorganisms. This model differs significantly from the many industrial methods that have been proposed for CO_2 sequestration. Other environments where this process may be occurring naturally include the playas at Salda Gölü in southwestern Turkey (Braithwaite and Zedef, 1994; Braithwaite and Zedef, 1996; Russell et al., 1999) and the hydromagnesite–magnesite playas of the Cariboo Plateau in British Columbia (Renaut, 1990, 1993).

The aim of this study is to characterize the hydromagnesite playas near Atlin and their surrounding environment in the context of a natural model for CO_2 sequestration with emphasis on microbial processes that accelerate mineral carbonation. This is accomplished by examining soil–microbial–bedrock interactions in the weathering regime, tracking the movement of carbon, and determining the genesis of the playas.

2. Background and general description of study area

Atlin is located in northwestern British Columbia, Canada (59°35′ N, 133°42′ W) at an elevation of 674 m. The area is situated in the Teslin Plateau ecosection, which is characterized by rolling hills and high plateaus with several large lakes (e.g., Atlin Lake) in wide valleys. This ecosection lies in a distinct rain shadow and has a dry sub-arctic climate. The yearly average temperature in Atlin is 0.5 °C with January (−15.4 °C) and July (13.1 °C) having the coldest and warmest average temperatures of the year, respectively. Precipitation (348 mm/yr) includes an average of 193 mm of rainfall and 155 mm of snowfall per year (Environment Canada). The Teslin Plateau ecosection is further subdivided into three biogeoclimatic zones. These include an alpine tundra zone (Boreal Altae Fescue Alpine) that is present on middle to upper slopes of most mountains, a spruce–willow–birch zone in high valleys and middle slopes, and a boreal white and black spruce zone that occurs throughout valley bottoms (British Columbia Ministry of Forests and Range). In this study, the role of bioweathering of ultramafic rock is examined on the slopes of Monarch Mountain near the town of Atlin.

The bedrock in this area is generally ultramafic and represents a tectonically emplaced upper mantle section of oceanic lithosphere consisting of an ophiolitic assemblage that formed during the Early to Middle Jurassic. The rocks are mainly serpentinized harzburgite with variable serpentinized, carbonitized, and deformed harzburgite, and with minor dunite lenses and pyroxenite veins (Hansen et al., 2005). The weathering of ultramafic bedrock in the Atlin area is reflected in the geochemistry of various waters that have been sampled and analyzed in this study.

In topographic lows near the town of Atlin, glacio-fluvial materials underlie two groups of playas that have a total area of approximately 11 ha (Young, 1916). In this study, these two groups are referred to as the northern and southern playas. The southern group consists of two playas, referred to as the southwestern and southeastern playas. Fig. 1 shows the locations and general shapes of each playa; aerial photographs of the northern and southeastern playas are shown in Fig. 2. This study is mostly concerned with the southeastern playa where present-day groundwater discharge forms a small wetland. As seen in Fig. 3, this playa area is subdivided into four terrains: wetland, grassland, localized (metre-scale) and amalgamated (decametre to hectometre-scale) hydromagnesite mounds.

3. Methodology

3.1. Monarch Mountain soil analyses

To examine the onset of (bio)weathering of magnesium silicates, a sample of serpentinite, collected from an outcrop in the southeastern playa, was cut into cubes (~1 cm^3) and polished on one

Fig. 1. Topographic map of the Atlin region. Water sampling locations (labels A to Q) correspond to those in Table 2, which lists the chemical data of each sample. The geology of the Atlin area, shown on the map, was documented and described by Ash and Arksey (1990). Groundwater flow to the playas is generally from the north and north-northeast (arrows). The soil sampling location on Monarch Mountain is marked by a star. (after Energy, Mines, and Resources Canada).

surface. Four cubes were placed in the organic horizon (~5 cm deep) on a slope of Monarch Mountain with the polished surface facing upward. The location is shown as a star on Fig. 1. The cubes remained buried in the soil for three years. On retrieval, they were placed in sterile 50 ml plastic vials, gently packed with soil, and were examined in the laboratory using scanning electron microscopy (SEM).

A soil profile was dug and sampled to characterize the soil near the location where the cubes had been buried. The profile was approximately 60 cm deep and extended to bedrock. Field observations of the soil including colour, grain size, and horizon thicknesses were recorded for soil classification. Soil samples were collected using a spatula rinsed in ethanol (70% $_{(aq)}$) at ~5 cm depth intervals, placed in sterile plastic bags, and stored at 4 °C until processed. In the field, a portion of each sample was used to prepare a slurry (50% soil by volume) with distilled water to measure pH using a Thermo Scientific Orion 4-Star Portable pH/ISE meter.

In the laboratory, each soil sample was enumerated for viable heterotrophic bacteria using the spread plate method. Serial dilutions were initiated by aseptically transferring aliquots (1.0 g) of soil to 9 ml of 0.85% NaCl solution and mixed by vortexing for 20 s. Sequential aliquots (1.0 ml) were transferred through the dilution series. One hundred microlitres of the appropriate dilutions were inoculated onto R2A (Difco®) agar plates in duplicate. Colony-forming units (CFU) were counted after an incubation period of one week at room temperature (~21 °C).

Samples collected every 10 cm were analyzed for their percent carbon (by weight) and stable carbon isotopes of the organic matter. Samples were dried at 60 °C for one day before being ground to a fine powder using a mortar and pestle. A method, modified from Verardo et al. (1990), was used to remove any potential pedogenic carbonate. Each sample was made moist with several drops of deionized water before reacting with 1.0 ml of sulphurous acid (6.4% SO_2). No effervescence was observed upon adding the acid. Samples were allowed to react for 2 h before being placed on a hotplate (~60 °C) to

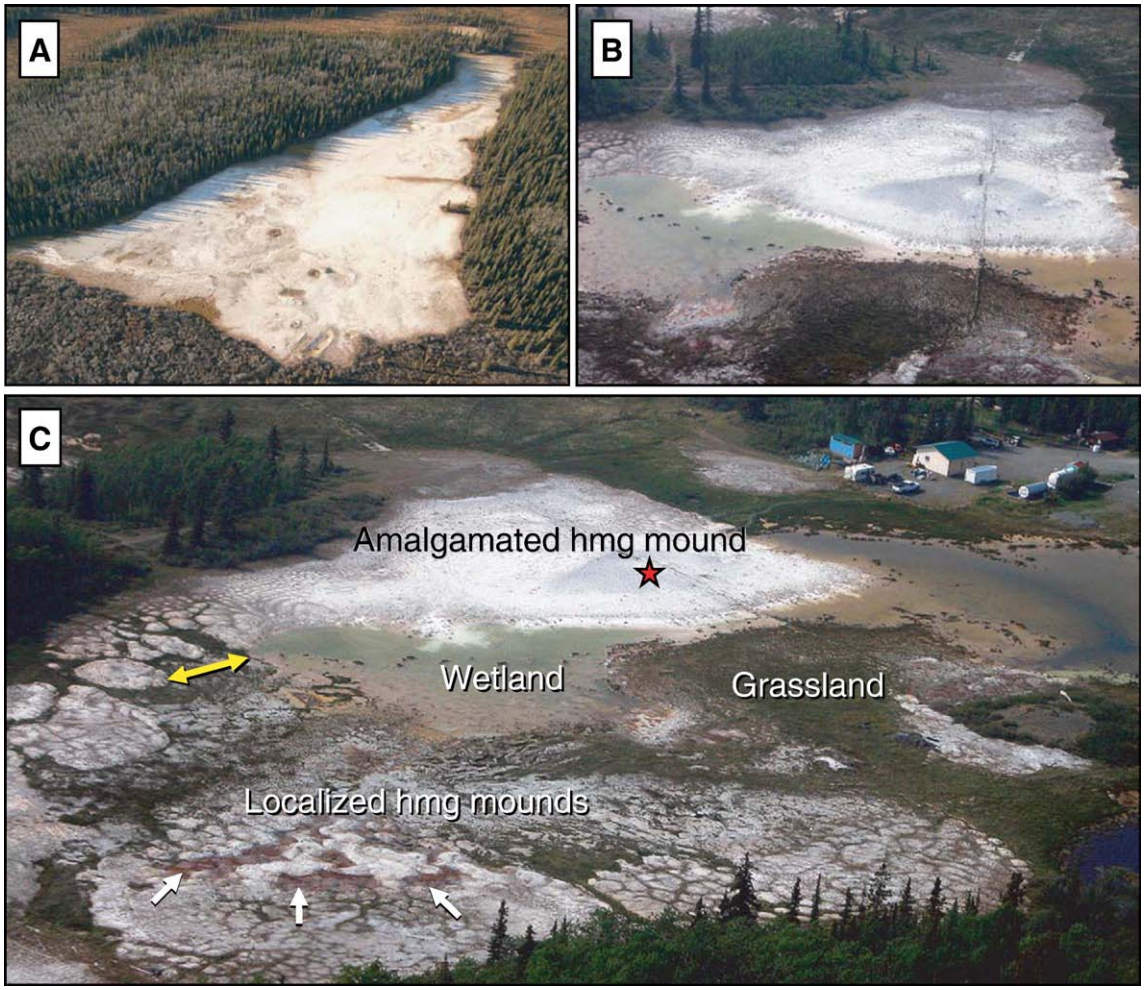

Fig. 2. A: Aerial photographs of the northern playa (facing north-westerly; Courtesy of Discovery Helicopters Ltd.) and sections of the southeastern playa (B: facing westerly and C: north-westerly). The locations of the grassland transect survey and hydromagnesite (hmg) mound core are marked with a line and star, respectively. Three arrows indicate areas of consolidated aragonite sediments surrounded by localized hmg mounds.

evaporate the sulphurous acid. A second treatment was conducted in the same manner to ensure complete removal of carbonate. A Fisons 1108 elemental analyzer was used to determine the percent of organic carbon. Soil standards of low (1.5% C) and high (6.2% C) organic content were used for calibration. A Costech Instruments' elemental combustion system, connected to a Thermo Finnigan DeltaPlus XL, was used to determine the carbon isotope composition relative to Vienna Pee Dee Belemnite (VPDB). An analytical precision of ±0.1‰ is estimated from repeated analysis of keratin (24.06‰), ANU-sucrose (−10.50‰), and NBS-22 (−30.00‰). Untreated portions of the same

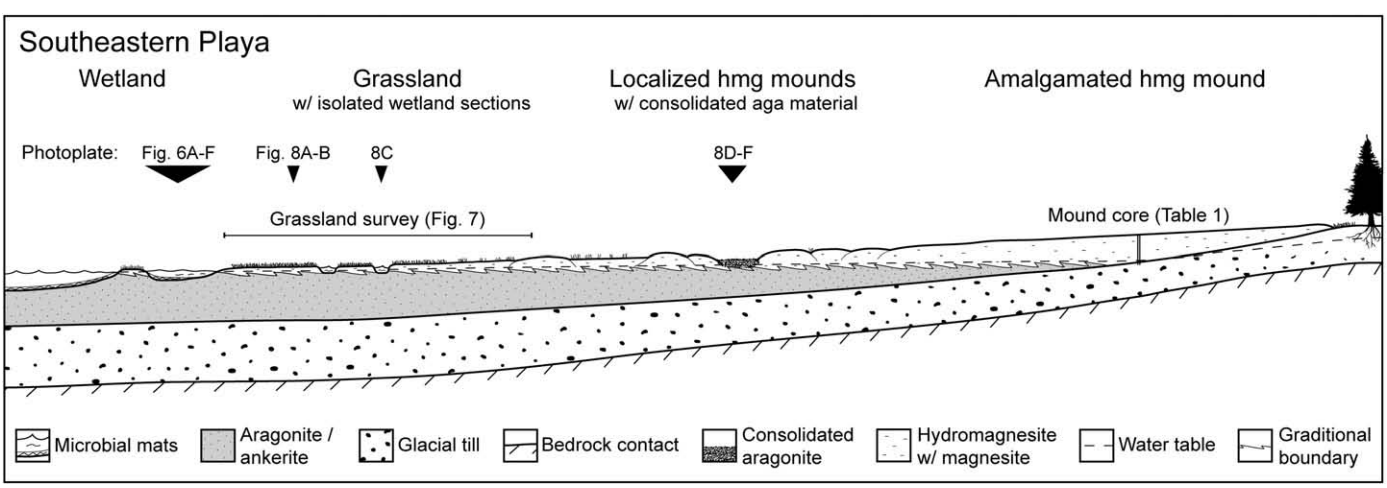

Fig. 3. Idealized cross-section of the southeastern playa. This playa can be divided into four terrains: wetland, grassland, localized and amalgamated hydromagnesite mounds. Conceptually, the locations of the grassland transect survey, hydromagnesite mound core, and photographs in Figs. 6 and 8 are labelled on the schematic.

samples were analyzed for their major elemental compositions using a Philips PW-1480 wavelength dispersive X-ray fluorescence (XRF) spectrometer.

3.2. Hydrogeochemistry

Numerous water bodies in the Atlin region were sampled to survey the water chemistry. In the field, pH was measured with a Thermo Scientific Orion 4-Star Portable pH/ISE meter and alkalinity was determined by titration with 0.1 M HCl (Lahav et al., 2001). Water samples for cation analyses were filtered (0.45 μm) in the field into sterile 15 ml plastic vials and acidified using concentrated nitric acid to obtain a pH of ~2. For anion and stable isotope analyses, samples were filtered (0.45 μm) into 125 ml polyethylene bottles and 2.0 ml glass vials, respectively. Groundwater was sampled from a well (59°34′40″ N, 133°41′70″ W) that is located approximately 20 m from the southeastern playa. The well (~35 m deep and 15.2 cm wide) was flushed with a minimum of three volumes to obtain representative groundwater. Filtered groundwater was dispensed into TraceClean™ 40 ml amber borosilicate vials with a 0.125″ septum liner for radiocarbon dating. All samples were stored at 4 °C prior to processing.

In the laboratory, cations and anions were analyzed using a Perkin-Elmer Optima 3300DV inductively coupled plasma-atomic emission spectrometer (ICP-AES) and Dionex IC-3000 ion chromatograph (IC), respectively. All blanks of deionized water were below detection limits for cations (ICP-OES) and anions (IC). Charge balances and saturation indices were determined from speciation calculations using PHREEQC (Parkhurst and Appelo, 1999). Radiocarbon analysis of the groundwater sample by Accelerator Mass Spectrometry was performed at the Isotrace Laboratory at the University of Toronto (Beukens et al., 1986).

Stable carbon isotopic compositions of dissolved inorganic carbon (DIC) in water samples from Atlin were determined using a Finnigan DeltaPlus XL mass spectrometer in continuous flow mode with a Gasbench device and A200s autosampler at the Pacific Centre for Isotopic and Geochemical Research in the Department of Earth and Ocean Sciences, The University of British Columbia. Four to five drops of 99% phosphoric acid were loaded in exetainer vials, sealed with a rubber septum, and flushed with helium for 5 min. A syringe was used to add 600 μl of the water sample. The exetainer was then shaken and left to react for a minimum of 1 h at 25 °C. The isotopic composition of the evolved headspace gas was measured in a helium flow. The external precision (1 sigma deviation) for isotopic analyses is <0.1‰ $\delta^{13}C$, as estimated from repeated analysis of in-house calcite standards and NBS-18 and NBS-19. At least three standards were analyzed for every eight samples. The results are reported using the δ notation measured in ‰ relative to Vienna Pee Dee Belemnite (VPDB).

3.3. Selective sampling from the southeastern playa–wetland

Selective sampling of the southeastern playa was conducted where groundwater discharge forms a wetland. Three key samples were collected from this location: (1) black, anoxic sediments (depth >5 cm), (2) benthic microbial mat and, (3) evaporative crusts that are common along the periphery of the wetland. A 70% (v/v) ethanol-rinsed spatula was used to place these samples into sterile 15 ml plastic vials. A sub-sample of the benthic microbial mat, overlying the anoxic sediments, was fixed in natural water using 2% (v/v) glutaraldehyde. These samples were examined using SEM and sub-samples were used to determine the mineralogy and stable isotope compositions ($\delta^{13}C$ and $\delta^{18}O$).

3.4. Grassland transect and hydromagnesite mound surveys

A grassland section of the southeastern playa was sampled along a transect line (35 m) at 5.0 m intervals, beginning at a localized hydromagnesite mound (metre-scale; referred to as ATC1) and extending to the perimeter of the wetland. The location of the transect line is shown in Fig. 2C. At each of the eight sampling points, a surface sample (0–5 cm depth) was collected and an auger was used to sample at various depths down to and below the water table. Samples were dried of excess water using Whatman® No. 1 filter paper to minimize the formation of evaporative minerals that might have formed after sampling. These samples were analyzed for their isotopic ($\delta^{13}C$ and $\delta^{18}O$) and mineralogical compositions. The pH of the water table was measured at each sampling hole using a Thermo Scientific Orion 4-Star Portable pH/ISE meter. A water sample was collected from a hole dug along the transect line at a distance of 18.5 m from the wetland margin for the analysis of cations, anions, alkalinity, and stable carbon isotopes of the DIC. In addition, a sample of grass was collected and analyzed for its $\delta^{13}C$ in the same manner described for the Monarch Mountain soil samples.

A sediment core (~67 cm deep) was taken from an amalgamated hydromagnesite mound adjacent to the wetland in the southeastern playa. The location of this core is shown as a star in Fig. 2C. Ten samples were collected along the core in plastic bags and later analyzed for whole rock geochemistry, isotopic composition ($\delta^{13}C$ and $\delta^{18}O$), and mineralogy by X-ray powder diffraction. Whole rock analyses were conducted at the McGill University Geochemical Laboratories. Results and detection limits can be found in Table 1. Hygroscopic water (H_2O-) and water of crystallization (H_2O+) values were determined by Activation Laboratories Limited and have detection limits of 0.01%.

Crushed samples of ~200 μg in mass were analyzed using a Thermo Finnigan Delta Plus XL mass spectrometer with a Gasbench device at the Pacific Centre for Isotopic and Geochemical Research,

Table 1
Whole rock geochemistry of sediments collected from the hydromagnesite mound core at the southeastern playa

Depth (cm)	Composition (%)										Composition (ppm)				Composition (%)						
	SiO_2	TiO_2	Al_2O_3	Fe_2O_3	MnO	MgO	CaO	Na_2O	K_2O	P_2O_5	Cr_2O_3	Ni	V	Zn	LOI	Total	CO_2	H_2O-	H_2O+	Sum (volatiles)	Total
3.5	0.41	0.007	0.06	0.04	n.d.	41.7	0.07	0.28	0.03	0.018	25	n.d.	n.d.	n.d.	57.2	99.8	41.2	1.26	14.6	57.0	99.6
10.5	0.46	0.007	0.05	0.04	n.d.	41.9	0.08	0.15	0.01	0.018	20	4.0	n.d.	n.d.	57.0	99.8	40.4	3.07	14.1	57.5	100.2
17.5	0.32	0.005	0.04	0.03	n.d.	41.9	0.06	0.21	0.01	0.017	18	3.0	n.d.	n.d.	57.2	99.8	40.3	4.37	13.8	58.5	101.1
24.5	0.29	0.005	0.04	0.02	n.d.	42.1	0.07	0.17	n.d.	0.017	18	n.d.	n.d.	n.d.	57.1	99.8	40.3	1.04	14.2	55.5	98.2
31.5	0.30	0.006	0.03	0.03	n.d.	42.1	0.06	0.17	0.01	0.017	18	n.d.	n.d.	n.d.	57.2	99.8	40.1	2.53	14.0	56.7	99.3
38.5	0.29	n.d.	0.03	0.03	n.d.	42.1	0.06	0.18	n.d.	0.017	16	n.d.	n.d.	n.d.	57.2	99.9	39.9	4.46	14.9	59.3	102.1
45.5	0.27	0.004	0.02	0.02	n.d.	42.1	0.06	0.16	n.d.	0.017	n.d.	n.d.	n.d.	n.d.	57.2	99.8	39.3	1.89	14.4	55.6	98.2
50.5	0.30	0.005	n.d.	0.02	n.d.	42.3	0.08	0.14	n.d.	0.017	15	n.d.	n.d.	n.d.	57.1	99.9	39.3	2.04	13.6	54.9	97.8
52.5	0.50	n.d.	0.02	0.02	n.d.	42.0	0.05	0.15	n.d.	0.018	n.d.	n.d.	n.d.	n.d.	57.0	99.7	38.6	0.53	14.4	53.6	96.3
66.5	0.37	0.004	n.d.	0.02	n.d.	42.1	0.03	0.15	n.d.	0.019	n.d.	n.d.	n.d.	n.d.	57.2	99.9	37.9	5.10	15.5	58.5	101.2
	Detection limits (ppm)																				
	60	35	120	30	30	95	15	75	25	35	15	3	10	2	100						

Analytes not detected are indicated by "n.d.". Stable carbon and oxygen isotope data for these samples are displayed in Fig. 8C.

The University of British Columbia. Samples were loaded into vials, flushed with helium, and dissolved in 99% phosphoric acid at 72 °C for a minimum of 1 h. Evolved headspace gas was measured in a helium flow. The $\delta^{18}O$ compositions are given relative to Vienna Standard Mean Ocean Water (VSMOW) and $\delta^{13}C$ compositions relative to Vienna Pee Dee Belemnite (VPDB). The external precision (1 sigma deviation) for isotopic analyses is <0.2‰ $\delta^{18}O$ and <0.1‰ $\delta^{13}C$, as estimated from repeated analysis of in-house calcite standards and NBS-18 and NBS-19. At least three standards were analyzed for every eight samples. The $\delta^{18}O$ compositions of magnesium carbonate minerals were corrected for reaction with phosphoric acid using the fractionation values from Das Sharma et al. (2002).

3.5. Scanning electron microscopy

Samples that contained biomass (e.g., serpentinite cubes, benthic microbial mat) were dehydrated in an ethanol series (25, 50, 75, 100% × 3 for 30 min each), critical point dried (Tousimis, Samdri-PVT-3B), and placed onto 12 mm carbon adhesive tabs (EM Science). A Denton Vacuum Desk II gold-cathode sputter coater was used to apply a gold–palladium coating to reduce sample charging. A ZEISS 1540 XB field emission gun-scanning electron microscope (FEG-SEM), operated with an accelerating voltage of 5.0 kV, was used to examine the samples and produce high-resolution images. An Oxford Instruments' INCAx-sight energy dispersive spectrophotometer (EDS) was utilized for elemental analysis.

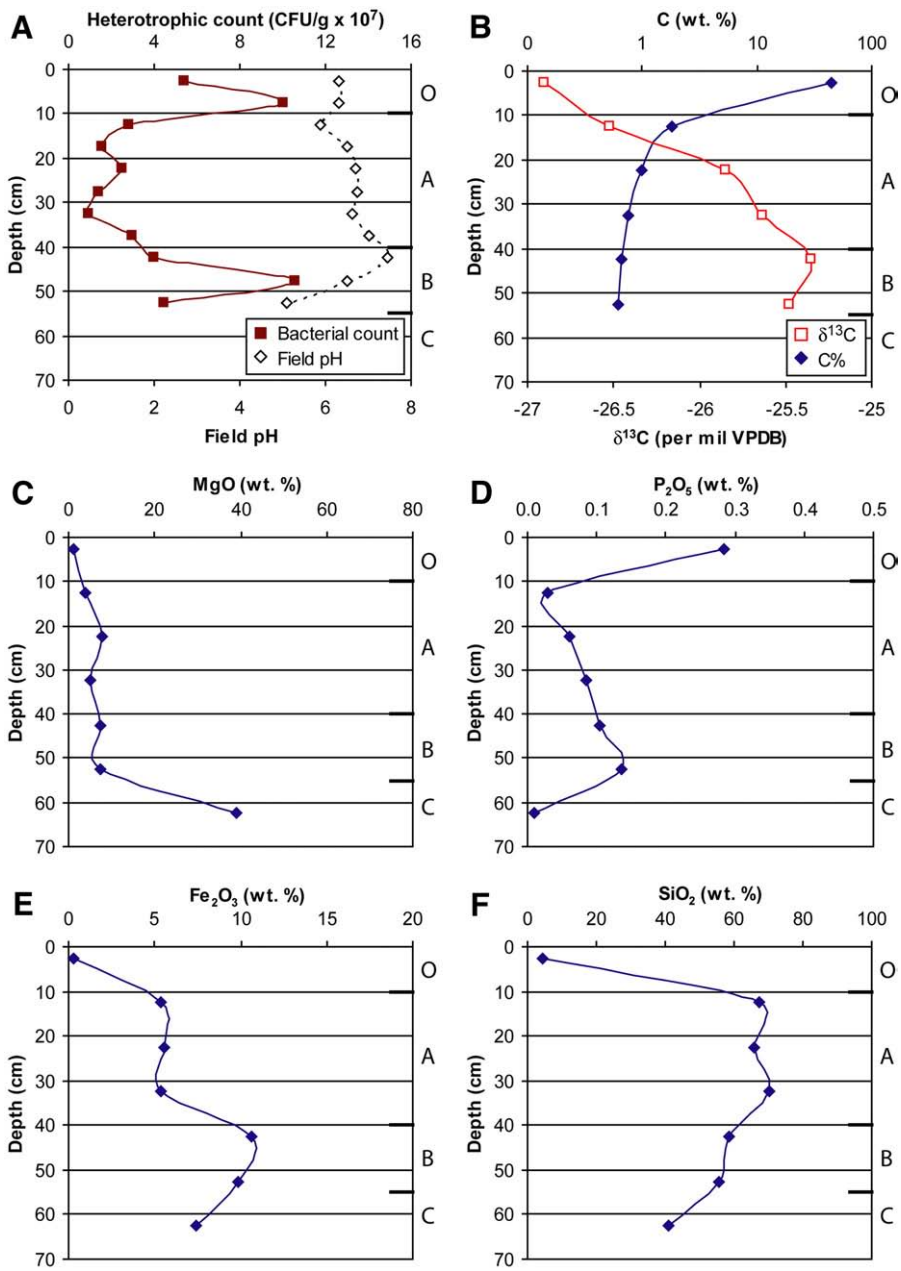

Fig. 4. Monarch Mountain soil data. The organic horizon, mineral horizons, and parent material are labelled on the secondary *Y* axis. A: Heterotrophic microbial counts ranged from 9.5×10^6 to 1.1×10^8 CFU/g while the pH value of the soil generally increased with depth. B: Carbon isotope values become enriched with depth as a result of microbial degradation of relatively depleted organic carbon. This is also reflected in the decreasing concentrations of organic matter with depth. C–F: X-ray fluorescence data for MgO, P_2O_5, Fe_2O_3, and SiO_2 in weight percent with depth.

3.6. X-ray powder diffraction

Step-scan X-ray powder-diffraction data were collected with CoKalpha radiation on a standard Siemens (Bruker) D5000 Bragg-Brentano diffractometer equipped with an Fe monochromator foil, 0.6 mm (0.3°) divergence slit, incident- and diffracted-beam Soller slits and a Vantec-1 strip detector. The long fine-focus Co X-ray tube was operated at 35 kV and 40 mA, using a take-off angle of 6°. Data were collected from 3–80° 2θ using a step size of 0.04° and a counting time of 0.8 s/step. The major crystalline mineral phases were identified with reference to the International Centre for Diffraction Data (ICDD) database using DIFFRAC^{plus} EVA (Bruker AXS, 2004). Semi-quantitative estimations of relative abundance of carbonate minerals were based on peak heights.

4. Results and discussion

4.1. Bioweathering of ultramafic rock

Over geological time, silicate weathering has been an important regulator of atmospheric CO_2 concentration (Holland et al., 1986) and may be accelerated by the production of chelating agents, and organic and inorganic acids produced by soil biota (Ullman et al., 1996). The high surface area of soils helps to retain moisture, thereby increasing the exposure time for acid attack (Schwartzman and Volk, 1989). In addition, the biota provides sinks for nutrients released by weathering and contributes to physical weathering through microfracturing (Schwartzman and Volk, 1989).

The soil sampling site on Monarch Mountain has bedrock composed mainly of harzburgite. Ash and Arksey (1990) describe harzburgite in the Atlin region as being green to black, with a rough, brown, weathered surface. The surface features of the bedrock are an expression of differential weathering, resulting from faster weathering of olivine and clinopyroxene and retention of the more resistant orthopyroxene. The bedrock is generally 20–60% serpentinized and characterized by preferential orientation of orthopyroxene grains. Soil formation is limited by the relatively dry, cool climate of the Teslin Plateau ecosection. The soil is sufficiently developed to exclude it from the Regosolic order, but has limited horizon development and may be partly disturbed either by plants or mass movement. The organic horizon is approximately 10 cm thick. The B horizon (15 cm thick) appears to be slightly altered by hydrolysis and oxidation, giving it a notably redder colour and finer grain size than the A horizon (30 cm thick). Based on visual examination of the soil profile and the compositional (XRF) data, this soil is classified as a Brunisol (Haynes, 1998). This soil type is poorly developed and is usually associated with forest vegetation.

The heterotrophic counts of the soil profile range from 9.5×10^6 to 1.1×10^8 CFU/g (Fig. 4A). There are relatively high bacterial populations at the top and bottom of the profile. This can be attributed to the presence of abundant organic matter in the organic horizon (top) and possibly the greater surface area of clays at the bottom. The organic horizon contains 44% organic matter, whereas, in the mineral horizons, organic carbon decreases from 1.8% (at 12.5 cm depth) to 0.63% (52.5 cm depth) as a result of degradation of organic matter over time (Fig. 4B). The microbial degradation of organic matter can be traced indirectly by the gradual increase in $\delta^{13}C$ values with depth (Fig. 4B). This is a result of fractionation that occurs as soil microbes preferentially consume ^{12}C-organics (Webb et al., 2004; Mora and Raich, 2007). The degradation of organic matter by microbes and respiration by plants greatly increases the partial pressure of CO_2 in soil to an estimated 10–100 times greater than atmospheric levels. This can result in weathering rates that are 2–6 times greater than those of bare rock under similar environmental conditions (Schwartzman and Volk, 1989). The concentration of CO_2 in sub-soils (B and C horizons) of a temperate forest can range from 1.5% in the dormant season to 5–7% during the growing season (Oh and Richter, 2004). However, organic acids are necessary to account for the observed present-day weathering rates because of the slow kinetics of proton production in the CO_2–H_2O system (Schwartzman and Volk, 1989). For example, oxalic acid producing fungi (e.g., *Aspergillus niger*) have been shown to degrade olivine, serpentine, muscovite, and feldspar (Burford et al., 2003). In the soil profile, indirect silicate mineral dissolution by the neutralization of inorganic and organic acids is reflected in a gradual increase in pH value with depth (Fig. 4A).

In addition to indirect microbial weathering caused by the production of acids, there is also direct microbially-aided silicate dissolution that occurs as microbes colonize mineral surfaces. Colonization of rock surfaces is advantageous to the soil biota because weathering releases essential nutrients (e.g., P, S) and metals (e.g., Na, K, Mg, Ca, Mn, Fe, Cu, Zn, Co, and Ni) that are vital to microbial and plant growth (Burford et al., 2003). Benzerara et al. (2005) investigated a pyroxene–carbonate–microbe interface using transmission electron microscopy and supporting techniques. They documented a 100 nm deep depression close to a microbe that had colonized a grain of orthopyroxene. Their results indicate that this feature resulted from microbially-mediated dissolution of the orthopyroxene. Benzerara et al. (2005) also noted the presence of nanometer-size crystals of calcite associated with the microbe, suggesting that carbonate mineralization had been mediated by the microorganism. The polished cubes in this study were notably weathered after burial in the soil on Monarch Mountain for three years. Both bacterial colonies (Fig. 5A) and isolated individuals are found heterogeneously distributed on the surface of the serpentinite. Cells commonly appear to be attached to the surface by films of extracellular organic matter. Areas of iron-rich minerals, possibly magnetite, are common on the polished surface and may be vulnerable to oxidation by iron-oxidizing bacteria (Ullman et al., 1996). In addition to bacteria, fungal hyphae extended across the polished faces (Fig. 5B). In soil, fungi play an

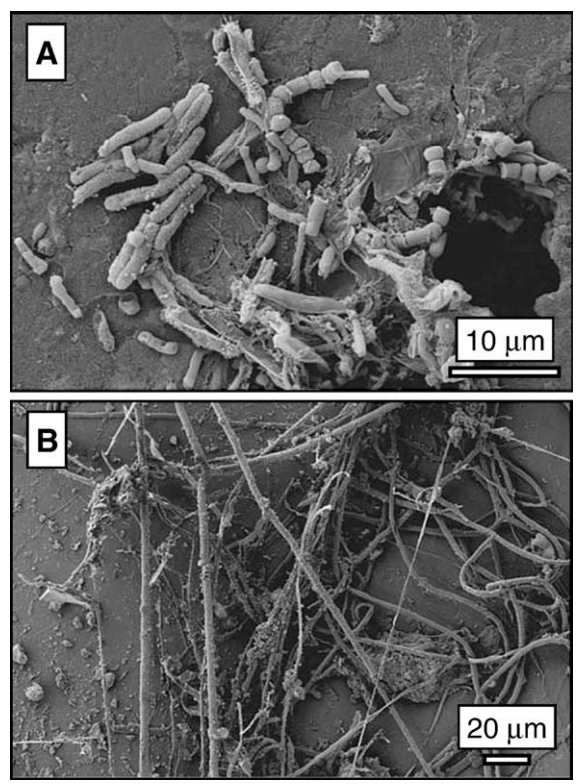

Fig. 5. Scanning electron micrographs of polished serpentinite cubes that were buried in the soil on a slope of Monarch Mountain for three years. A: Bacterial colony associated with a corrosion pit and B: fungi colonizing the serpentinite surface.

important role in carbon cycling and other biogeochemical cycles. They are present as filamentous forms, plant symbionts, unicellular yeasts and animal and plant pathogens. Fungi are ideally suited as biological weathering agents because of their filamentous growth habit and ability to produce organic acids, protons, carbonic acid, and other metabolites with chelating properties (Burford et al., 2003).

Fig. 4C–F displays total concentrations of selected metals (MgO, P_2O_5, Fe_2O_3, and SiO_2) for the soil profile (values given as weight-percent oxides). Silica accounted for 50–70% of the mass of the mineral horizons. This is notably higher than the 41% in the underlying parent material. Silica enrichment suggests preferential weathering of mafic minerals and eluviation of more mobile elements such as Mg (Starr and Lindroos, 2006). Concentrations of Fe_2O_3 show enrichment in the B horizon, further indicating eluviation–illuviation and coinciding with a rusted appearance at depth (40–55 cm). An enrichment of P_2O_5 in the O horizon, followed by a sharp depletion in the A horizon, attests to its biogenic origin. The MgO concentration ranges from 3.9–7.3% in the mineral horizons that are significantly depleted in comparison to the parent material (39%). The weathering of ultramafic rocks results in the release of magnesium, which becomes available for trapping carbon dioxide by forming carbonate minerals.

Schwartzman and Volk (1989) state that the stabilization of soil, combined with biological effects, can result in weathering rates that are at least 100 times greater (and perhaps >1000 times greater) than those of a purely abiotic rock surface. Their modelling demonstrated that if present-day weathering rates were not enhanced by a factor of 100 caused by biological activities, than a purely abiotic Earth would be 20–40 °C warmer. This is the result of the increase in mineral dissolution and the flux of dissolved inorganic carbon (DIC) from the continents (Andrews and Schlesinger, 2001). In this study, water flowing from a spring at the base of Monarch Mountain is notably enriched in Mg and DIC compared to surface waters on top of the mountain (e.g., NW pond and SE pond). Presumably, the increase in DIC is reflected by the alkalinity values in Table 2. On a watershed scale, the chemistry of the spring water reflects the weathering of the ultramafic minerals from the mountain.

4.2. Hydrogeochemistry

The magnesium-rich waters of the Atlin region are a direct result of the weathering of ultramafic and mafic bedrock. The topographic map in Fig. 1 shows the locations of each water sample, and its corresponding number, listed in Table 2. The analytical data collected for these waters include pH, alkalinity, $\delta^{13}C$ of DIC, and cation and anion concentrations.

Based on the surface topography, groundwater flows to the playas and associated wetlands from the mountains adjacent to Como Lake. The muddy substrate of Como Lake consists of aragonite, but lacks magnesium carbonate minerals, which are probably absent because of the low Mg/Ca ratio (~3:1) of the lake waters. A lake west of Como Lake has similar water chemistry, but with a lower pH and no visible carbonate sediments. As groundwater flows toward the playas it interacts with the rocks to the north, which have been previously described by Ash and Arksey (1990; Fig. 1). Metabasalt predominates in the areas where the groundwater originates. Serpentinite–bastite is the major rock type closer to the playas and outcrops of serpentinite are found in the southeastern playa. The serpentinite–bastite is an altered form of harzburgite that weathers to a light to dull grey colour and has a mylonitic fabric, with 1–3 mm black bands of bastite–serpentine (after orthopyroxene) in an antigorite–serpentine (after olivine) matrix (Ash and Arksey, 1990). In addition, it contains minor to moderate amounts of talc and accessory magnetite and carbonate minerals. Groundwater flow in the watershed is likely to follow carbonate-altered zones where dissolution of magnesite has a disproportionately greater influence on water chemistry, given its ease of weathering in comparison to that of silicate minerals. Most of the waters in the Atlin area that have been analyzed are supersaturated with respect to calcite, aragonite and magnesite and the wetland in the southeastern playa is also supersaturated with respect

Table 2
Atlin area water chemistry

	Sample location	pH	Alkalinity	$\delta^{13}C$ −DIC	Cation concentrations (mg/l)							Anion concentrations (mg/l)					Supersaturated phases
			mg/l HCO_3^-	‰ VPDB	Mg	Ca	Na	K	Fe	Al	Si	Cl	F	SO_4	NO_3	PO_4	
A	Como Lake	8.8	466	−1.5	87.8	26.5	5.71	2.95	n.d.	n.d.	5.21	3.76	n.d.	61.8	n.d.	n.d.	Mgs, Cal, Arg
B	Lake west of Como Lake	8.3	416	−7.6	60.2	59.4	3.45	6.63	n.d.	0.01	1.54	1.08	n.d.	68.0	n.d.	n.d.	Cal, Arg, Mgs
C	Wetland NW of N playa	8.2	423	−10.1	40.2	79.0	2.06	6.15	0.02	0.01	1.08	1.85	n.d.	14.9	n.d.	n.d.	Cal, Arg, Mgs
D	Northern playa wetland	8.3	1240	−11.3	209	60.9	5.49	15.9	n.d.	n.d.	1.06	0.67	n.d.	1.95	n.d.	n.d.	Mgs, Cal, Arg
E	Northern playa spring	8.0	3620	4.3	717	73.6	30.3	31.5	n.d.	n.d.	9.67	1.16	n.d.	65.7	n.d.	n.d.	Mgs, Cal, Arg
F	Groundwater from well near Southern playas 2005	8.0	2770	−6.8	353	5.00	16.0	6.81	0.04	0.0	7.48	2.24	n.d.	47.4	10.0	0.72	Mgs, Cal, Arg
	2007	8.2	2700	−6.8	526	n.d.	13.5	6.80	n.d.	n.d.	7.48	0.32	n.d.	39.1	n.d.	n.d.	Mgs
Radiocarbon analysis: $\delta^{13}C = -5.7$‰, 11.3 pMC																	
G	Southeastern playa–south wetland 2005	8.6	4730	5.2	575	10.2	96.3	23.7	0.05	0.0	15.9	10.9	n.d.	177	18.6	1.12	Mgs, Hmg, Cal, Arg
	2007	8.2	4960	1.5	1020	24.4	47.3	24.4	n.d.	n.d.	9.27	2.53	n.d.	113	n.d.	n.d.	
H	Isolated wetland	8.0	4320	2.2	921	n.d.	66.1	19.3	0.48	n.d.	10.4	1.35	n.d.	61.1	n.d.	n.d.	Mgs
I	Grassland transect survey	7.1	7300	−1.1	1270	54.7	48.4	41.1	n.d.	n.d.	6.84	0.31	n.d.	6.65	n.d.	n.d.	Cal, Arg
J	Atlin Lake	7.8	56.1	−5.3	3.20	14.6	0.79	1.10	0.01	0.01	0.64	0.22	0.06	6.12	n.d.	n.d.	
K	Atlin Lake inlet (mouth)	8.3	1100	−8.2	199	69.9	20.1	12.3	0.10	n.d.	2.67	34.2	n.d.	21.2	n.d.	n.d.	Mgs, Cal, Arg
L	Atlin Lake inlet (wetland)	8.2	868	−10.8	142	49.0	18.7	11.8	n.d.	n.d.	3.04	25.2	n.d.	13.4	n.d.	n.d.	Mgs, Cal, Arg
M	Wetland east of Southern playas	7.9	422	−8.8	87.7	13.0	0.73	15.6	0.21	0.04	0.59	1.61	n.d.	n.d.	n.d.	n.d.	Mgs
N	Pine Creek	7.9	65.1	−9.9	4.34	11.0	3.79	3.43	0.01	0.00	1.23	0.12	0.93	0.12	n.d.	n.d.	
O	Monarch Mt. spring	8.0	414	−13.2	49.5	33.2	3.96	5.58	0.01	0.01	1.67	0.54	0.07	0.52	n.d.	0.01	Cal, Arg, Mgs
P	Monarch Mt. NW pond	8.5	123	–	18.1	7.05	2.96	1.08	0.06	0.03	1.34	0.21	0.04	0.20	n.d.	0.02	Mgs
Q	Monarch Mt. SE pond	9.4	55.0	–	8.95	1.72	3.02	3.53	0.03	0.02	1.33	0.77	0.06	7.64	n.d.	0.01	Mgs

Dashes (–) and "n.d." indicate data not obtained and analytes not detected, respectively. Saturation indices (SI) for relevant mineral phases including aragonite (Arg), calcite (Cal), magnesite (Mgs), hydromagnesite (Hmg), and nesquehonite (Nes) were calculated using PHREEQC (Parkhurst and Appelo, 1999). Supersaturated phases are listed by SI in descending order.

to hydromagnesite. This is in part a result of the relatively closed nature of this water body that has resulted in evapoconcentration of dissolved magnesium.

The small wetland in the southeastern playa (59°34′30″ N, 133°41′60″ W) shows significant precipitation of carbonate minerals. It has an area of ~0.5 ha, an average depth of ~0.3 m, and no channelled inflows or outflows and is therefore presumably fed by groundwater. The groundwater sampled from a nearby well had a pH value slightly above 8 and an alkalinity of ~2700 mg/l HCO_3^-. Sodium and chloride analyses show that the wetland water is concentrated in these ions by approximately four to eight times relative to groundwater sources. The precipitation of magnesium carbonate minerals from the wetland water is reflected in an only two-fold increase in dissolved magnesium. Concentrations of other anions, such as Cl^- and SO_4^{2-}, are negligible and do not result in the precipitation of salts. The wetland is very alkaline (~4800 mg/l HCO_3^-), has a pH of 8.2 to 8.6, a Mg concentration as high as 1024 ppm, and a Mg/Ca ratio of approximately 50:1. These geochemical conditions are favourable for precipitating abundant magnesium carbonate minerals.

4.3. Southeastern playa–wetland

Characterizing sediment and microbial samples from the wetland in the southeastern playa highlights mechanisms that contribute to carbonate precipitation. As with weathering processes, the precipitation of carbonate minerals in this environment is mediated by both abiotic and biotic processes. In the wetland, anoxic black sediments are present beneath benthic microbial mats at a depth >5 cm (Fig. 6A–B). They consist of aragonite with iron sulphides that give the sediments a black colour. Groundwater discharging into the wetland is supersaturated in dissolved CO_2 and equilibrates with the atmosphere by degassing CO_2, which aids in precipitating aragonite. The absence of magnesium carbonates in these sediments may be caused by the relatively low pH value (~8.1) and the occurrence of iron sulphide minerals suggests the presence of sulphate-reducing bacteria (SRB). SRB have been implicated in dolomite precipitation (van Lith et al., 2003a,b) and may aid in the formation of aragonite in these sediments. Sulphate creates a strong ion pair with dissolved magnesium and is thought to inhibit dolomite formation (Baker and Kastner, 1981;

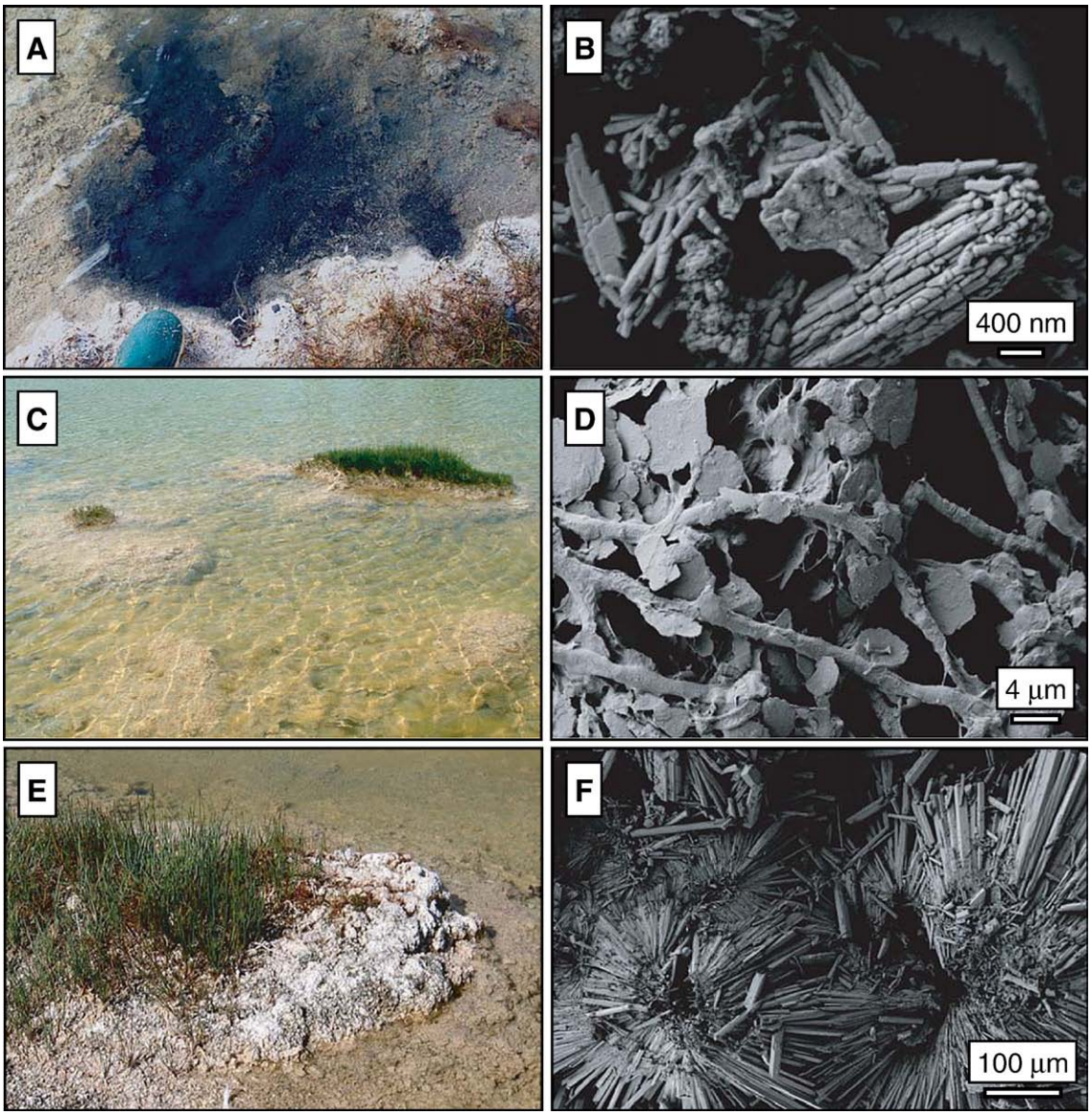

Fig. 6. Photographs and corresponding SEM micrographs of samples collected from the southeastern playa-wetland. A–B: Benthic mats in the wetland have been removed to show the aragonite sediments with black iron sulphides beneath. C–D: Benthic microbial mats and mounds that can emerge from the water surface to be colonized by grass. SEM micrograph flakey hydromagnesite and/or dypingite associated with filamentous cyanobacteria. E–F: An evaporative crust along the wetland margin. This nesquehonite crust appears as tightly bound radial arrangements of prismatic crystals (SEM micrograph).

Kastner, 1984). Intuitively, this may also be the case for other magnesium carbonate minerals. Sulphate reduction results in localized enrichment of bicarbonate, removal of sulphate as sulphide minerals precipitate, and an increase in pH value (van Lith et al., 2003b; Eq. (4)).

$$4CHO_2^- + SO_4^{2-} + H^+ \rightarrow 4HCO_3^- + HS^- \quad (4)$$

SRB may also aid in creating favourable geochemical conditions for the precipitation of magnesium carbonate minerals in the overlying benthic microbial mats.

A variety of biofilms and microbial mats containing filamentous cyanobacteria inhabit the wetland. Most prominent are the benthic microbial mats (Fig. 6C) that cover the wetland floor and overlie the anoxic black sediments. The mats are typically 5 cm thick, non-laminated and non-lithified, and have been shown to mediate magnesium and calcium carbonate precipitation (Power et al., 2007). They are greenish brown on the surface and greener underneath, consisting mainly of aragonite and dypingite [$Mg_5(CO_3)_4(OH)_2 \cdot 5H_2O$]. Fig. 6D shows platy dypingite associated with filamentous cyanobacteria in the mats. Although wetland water is supersaturated with respect to hydromagnesite, abiotic precipitation experiments by Power et al. (2007) demonstrated that only nesquehonite [$MgCO_3 \cdot 3H_2O$] precipitated after evaporation of wetland water. These authors used both field and laboratory experiments to demonstrate that filamentous cyanobacteria can promote the precipitation of dypingite and aragonite from wetland and groundwater collected from the Atlin site.

Cyanobacteria are able to overcome kinetic barriers and induce precipitation of carbonate minerals. The interstitial water in their microenvironments can become dramatically altered relative to ambient water by their biological processes and produce geochemical conditions that favour carbonate precipitation. For instance, photosynthesis results in the alkalization of this microenvironment by removing bicarbonate and generating hydroxyl anions (Thompson and Ferris, 1990; Pentecost, 1995; Riding, 2006; Eq. (5)).

$$HCO_3^- + H_2O + hv \rightarrow CH_2O + OH^- + O_2\uparrow \quad (5)$$

Increased hydroxyl activity promotes the formation of both dypingite and hydromagnesite (Power et al., 2007). In addition, microbial cell walls provide an ideal surface for mineral nucleation with large numbers of regularly-spaced, chemically-identical nucleation sites (e.g., carboxyl groups and amino functional groups). Microbial cell walls also concentrate cations, such as Mg^{2+} and Ca^{2+}, from solution as a result of a net-negative surface charge (Braithwaite and Zedef, 1996; Schultze-Lam et al., 1996; Obst et al., 2006; Eq. (6)). These adsorbed cations may then act as salt bridges for attracting bicarbonate and carbonate anions (Braithwaite and Zedef, 1996). The geochemical conditions that result from these microbial processes favoured the precipitation of dypingite ($Mg_5(CO_3)_4(OH)_2 \cdot 5H_2O$; Eq. (7)) in the wetland.

$$R.COO^- + Mg^{2+} \rightarrow R.COOMg^+ \quad (6)$$

$$5Mg^{2+} + 4CO_3^{2-} + 2OH^- + 5H_2O \rightarrow Mg_5(CO_3)_4(OH)_2 \cdot 5H_2O \quad (7)$$

The biologically-mediated formation of dypingite in this system likely serves as a precursor to the formation of hydromagnesite via dehydration. The wetting and drying cycles, experienced by the playas, provide the appropriate environment for this dehydration reaction to occur.

Similar to the southeastern playa–wetland, Braithwaite and Zedef (1996) found that precipitation of hydromagnesite from Salda Gölü (Lake) in Turkey was microbially-driven. Magnesium concentrations at Salda Gölü (~200 ppm) are notably lower than those in the southeastern playa–wetland near Atlin and demonstrate that

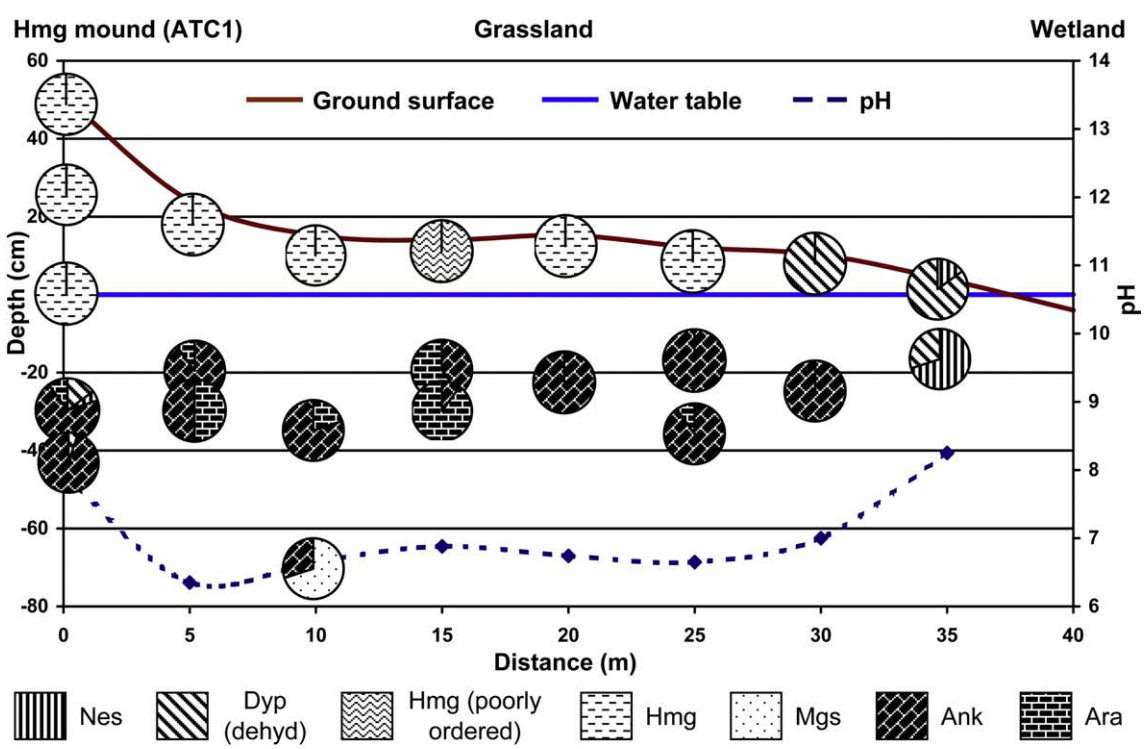

Fig. 7. Graph showing samples from the grassland transect survey beginning at a hydromagnesite mound (ATC1) and extending to the wetland perimeter. Pie diagrams display the semi-quantitative proportion of the minerals for each sample determined using XRD data. The ground surface is the top solid line and the water table (assumed level) is shown as a horizontal solid line. Near wetland sediments are composed of evaporative crusts of nesquehonite and dypingite that formed in association with microbial mats that were previously part of the wetland. Hydromagnesite is the dominant mineral phase in sediments that are above the water table whereas ankerite and aragonite are common below the water table.

hydromagnesite may precipitate, with the aid of microbes, in waters that are geochemically undersaturated with respect to hydromagnesite.

Diatom species of *Navicula* and *Cyclotella* are common in this wetland and are sinks for dissolved silicon (Power et al., 2007; Renaut, 1993). Although sepiolite [$Mg_4Si_6O_{15}(OH)_2 \cdot 6H_2O$] is supersaturated in this wetland and in other water bodies in the Atlin area, it has not been detected in any of the sediment samples analyzed by XRD. The abundance of diatoms in this wetland and perhaps others may be minimizing or preventing the precipitation of magnesium silicate clays by significantly decreasing silicon concentrations. The presence of large populations of diatoms eliminates a potential non-carbonated sink for magnesium (i.e., Mg-silicate clays).

Over long periods, carbonate sediments fill the water bodies that occupy the topographic lows and the key process for the precipitation of carbonate minerals shifts from being a biologically-aided process to one driven by evaporation. For example, centimetre-scale crusts of nesquehonite are common on exposed surfaces adjacent to the water body (Fig. 6E–F). In these crusts, nesquehonite forms as aggregates of slender prismatic crystals that radiate from a central point. Experimental studies have shown that nesquehonite can precipitate in drying cyanobacterial mats (McLean et al., 1997; Zaitseva et al., 2007).

4.4. Southeastern playa–grassland

As the wetland fills, grasses colonize exposed sediments forming a grassland terrain, which can be considered an emerged wetland (Fig. 3). No microbial mat structures are preserved in the grassland sediments. Microbial mats associated with magnesium carbonate sediments have a low preservation potential in regards to forming a microbialite (a fossilized microbial-sedimentary structure; Renaut, 1993). Several factors, including desiccation, cryogranulation, interstitial carbonate precipitation, recrystallization, bioturbation, compaction, and erosion can contribute to poor preservation (Renaut, 1993).

Fig. 7 shows the mineralogy of 23 sediment samples collected along the grassland transect line that extends from a localized hydromagnesite mound (ATC1) to the wetland perimeter. Each pie diagram represents a sample analyzed by XRD. The relative abundances of

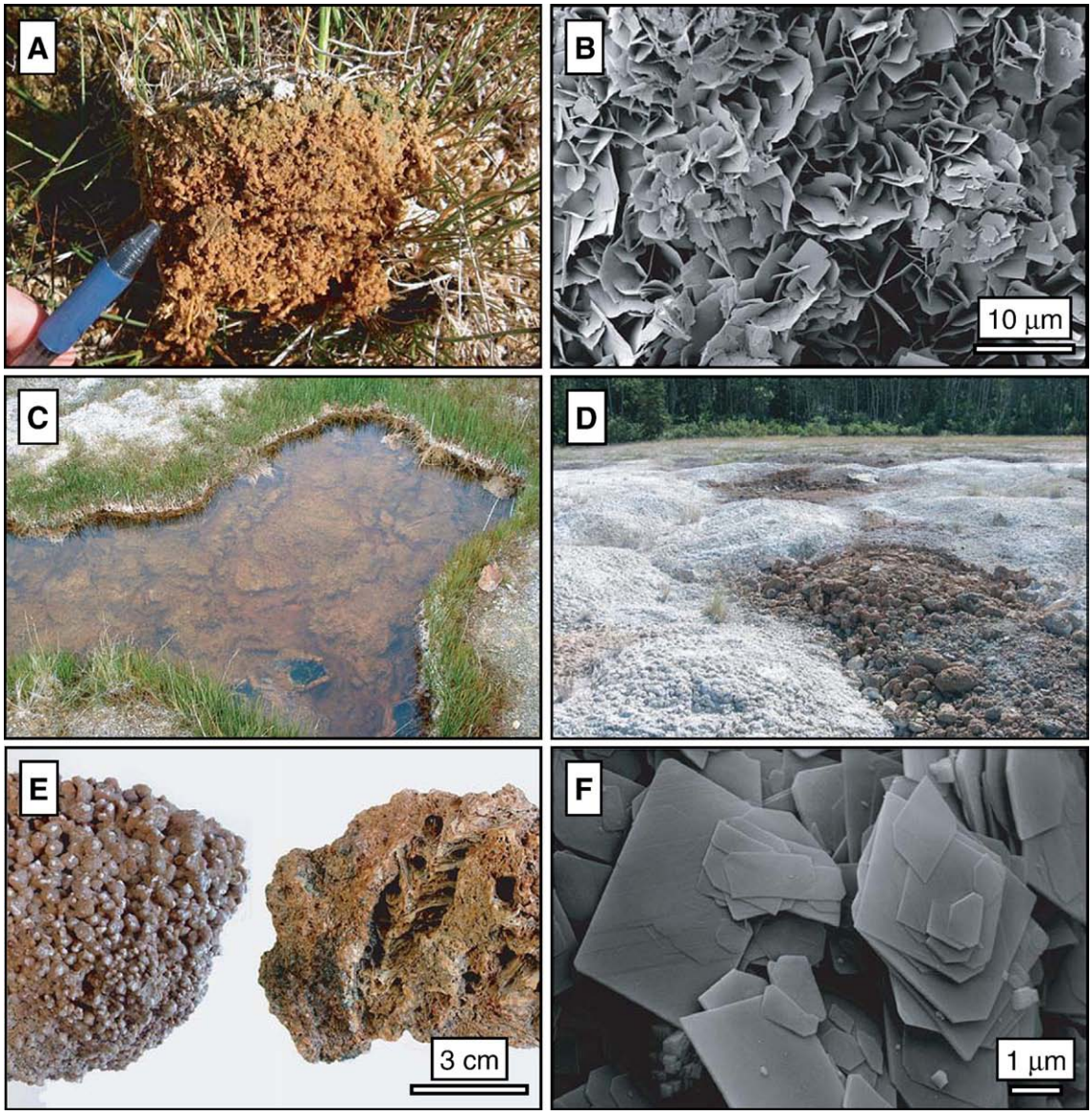

Fig. 8. Photographs and SEM micrographs of samples from the southeastern playa. A–B: Near surface sediments from the grassland, adjacent to the wetland, showing radiating aggregates of plate-like hydromagnesite crystals. C: Isolated wetland section showing well-defined boundaries and containing iron-stained microbial mats. D: Localized hydromagnesite mounds surrounding well-defined patches of iron-stained, gravel-like aragonite. E: Hand specimens of a pisolite with inverse grading and possibly a fossilized microbial mat exhibiting alveolar–septal structures. F: SEM micrograph of the hydromagnesite found in the mounds showing platy crystal morphology.

mineral phases were estimated from the peak heights of the XRD patterns. Near the perimeter of the wetland, sediments mainly consist of nesquehonite and partially dehydrated dypingite. This is consistent with nesquehonite forming at the surface of the water and on exposed surfaces as an evaporite and with dypingite forming within the microbial mats (McLean et al., 1997; Power et al., 2007). In addition, there is considerable iron staining in subsurface sediments that are directly adjacent to the wetland. Further from the wetland, hydromagnesite is dominant above the water table. The hydromagnesite is granular, lightly stained with iron oxides, and consists of aggregates of plate-like crystals (Fig. 8A–B). The hydromagnesite in the central region of the transect is poorly ordered, suggesting further dehydration of dypingite to form hydromagnesite. Hydromagnesite that is in the mound (ATC1) is well-crystallized. Ankerite [$Ca(Fe^{2+},Mg,Mn^{2+})(CO_3)_2$] and aragonite are common below the water table. A number of the samples containing ankerite have considerable proportions of amorphous material (or poorly crystalline) as seen by a broadening of the XRD peaks. The pH of the water below the surface of the water table ranges from 8.3 near the wetland to <7 throughout the middle section of the transect and 7.9 below the hydromagnesite mound (ATC1). This likely relates to generation of alkalinity by photosynthesis within the wetland (Thompson and Ferris, 1990) and of acidity by decomposition of organic matter within the sediments of the grassland. The pH of the groundwater below the hydromagnesite mound (ATC1) is relatively high (7.9) in the absence of significant microbial degradation of organic matter.

In the grassland terrain, sections of wetland become relatively isolated as the main wetland fills with sediment (Fig. 8C). These residual areas have microbial mats and pH values (8.0) that differ considerably from those in the main wetland. The mats are stained by iron and in some cases appear to have microbially formed alveolar-septal structures (Hillgärtner et al., 2001). The precipitation of aragonite dominates within these small water bodies. Further from the main wetland and between localized hydromagnesite mounds there are patches of consolidated aragonite sediments (Fig. 8D). This material includes pisolites with inverse grading and possibly fossilized microbial mats (Fig. 8E). Diatoms can be seen in petrographic thin sections of the hand specimen shown on the right of Fig. 8E. The similarities between the contemporary isolated wetland sections and the well-defined patches of consolidated material strongly suggest that present-day conditions are similar to those of the past.

4.5. Southeastern playa–hydromagnesite mounds

The localized metre-scale mounds of hydromagnesite that surround patches of consolidated aragonite sediments are shown in Figs. 2 and 8D. These semi-circular mounds have distinct boundaries with characteristic cauliflower surfaces that are made up of small aggregates (5–10 cm) formed by expansion and contraction during subaerial drying (Stamatakis et al., 2007). Sediments, below the mound at the beginning of the grassland transect line (ATC1; Fig. 7), are mainly composed of ankerite, suggesting that the hydromagnesite mounds form on top of the grassland sediments.

The development of localized hydromagnesite mounds results from differences in grain size of the substrate. The coarse consolidated aragonite sediments do not allow for the capillary rise of groundwater. In contrast, the capillary rise of Mg-rich water through the muddy grassland sediments would evaporate at or near the surface to produce fine-grained precipitates and cause the mounds to grow. Precipitation of carbonate minerals near the surface coupled with erosion causes localized mounds to grow and flatten over time, resulting in the amalgamation of these mounds into larger mounds. Over time, this process will cause the southeastern playa to resemble the northern playa, where presently there are no wetland or grassland terrains (Fig. 2A). Furthermore, consolidated aragonite sediments have been found partially buried in the hydromagnesite sediments in the northern playa and suggest that it originally had similar depositional environments to the present-day southeastern playa.

The amalgamated hydromagnesite mounds have sharp boundaries and minor relief compared to the surrounding land. As previously described, the raised surfaces of the mounds are caused by the upward movement of water by capillary action. The sediments, containing hydromagnesite and magnesite, are generally homogeneous with only a faint horizontal parting (~0.5 cm) emphasized upon desiccation. The hydromagnesite crystals in the mounds appear as stacks of plates (Fig. 8F) as opposed to radiating aggregates of plate-like crystals seen in the grassland sediments. The hydromagnesite is bright white and in bulk ranges from powdery to clay-like, depending on the water content. At depth, it has a yellow tinge that may be from the presence of detrital minerals or iron oxides.

The northern and southern playas have large hydromagnesite mounds that have been described previously by Young (1916). The northern playa (7.3 ha) is the largest and has a number of small satellite playas with a total area of 0.8 ha. The southwestern (total area = 0.4 ha) and southeastern (total area = 2.1 ha) playas are separated by a bedrock ridge. These estimates only include the bright white hydromagnesite found in the amalgamated mounds. Young (1916) estimated an overall area of ~106,000 m^2 and average thickness of 0.8 m. He estimated there to be 163,000 tons of material, mainly hydromagnesite with minor amounts of magnesite, using an average density of 1.84 g/cm^3. Grant (1987) based his analysis on Young (1916) and gives approximately the same areas and average depths, but calculates an overall mass of only 116,000 tons. This disparity is likely a difference in assumed densities, possibly dry vs. wet density, used to calculate the mass.

Table 1 contains the whole rock geochemical data for the core samples collected from the hydromagnesite mound of the southeastern playa. On average, the sediments contain 42.0% MgO and 57.1% volatiles (CO_2 and H_2O). The mounds consist mainly of hydromagnesite (ideal composition = 43.1% MgO, 37.6% CO_2, and 19.3% H_2O) and minor amounts of magnesite (ideal composition = 47.8% MgO and 52.2% CO_2). The MgO:CO_2 ratio increases with depth and the percentage of CO_2 decreases with depth. Both of these trends indicate a greater portion of magnesite (1:1 MgO:CO_2) near the surface. This is likely caused by desiccation of the sediments at and near the surface during the summer months.

4.6. Carbon and oxygen isotopes

One aspect of this study involves understanding the movement of the carbon that is ultimately sequestered within carbonate minerals in the playas. This has been accomplished in part by analyzing the isotopic compositions of the various carbon-bearing materials in the weathering regime and across depositional environments. The three major carbon sources that contribute to precipitation of carbonate minerals at Atlin are: (1) atmospheric CO_2, (2) soil organic matter (SOM) from groundwater recharge zones, and (3) dissolved bedrock carbonate (e.g., magnesite) introduced by groundwater prior to discharge into ponds and wetlands associated with the playas. The SOM of the organic horizon sampled on Monarch Mountain had a $\delta^{13}C$ value of −26.9‰, signifying organic matter derived from C_3 vegetation (Fairchild et al., 2006). In general, soil CO_2 is slightly ^{13}C-enriched relative to SOM because of the diffusion of atmospheric CO_2 into the soil (Bowling et al., 2008; Flanagan et al., 1996). The $\delta^{13}C$ and $\delta^{18}O$ values for the carbonate minerals in the magnesite-, talc-, and quartz-zones of the listwanite (carbonated serpentinite) near Atlin range from approximately −7 to −1‰ VPDB and from approximately 6 to 16‰ VSMOW, respectively (Hansen, 2005).

Typical groundwater has $\delta^{13}C$ values ranging from −30 to 0‰, with the most common values falling between −25 and −10‰ (Boutton, 1991). Groundwater from the well near the southeastern playa has an average $\delta^{13}C$ value of −6.44‰ (three analyses). Intuitively, the

significantly greater dissolution rate of listwanite in comparison to Mg-silicate minerals would suggest a large portion of groundwater DIC originates from bedrock carbonate. A simplified chemical reaction between carbonic acid and magnesite indicates that one half of the bicarbonate produced originates from magnesite (Eq. (8)).

$$MgCO_3 + H_2O + CO_2 \rightarrow Mg^{2+} + 2HCO_3^- \quad (8)$$

However, based on a mixing model of the two dominant carbon sources in groundwater, soil CO_2 ($\delta^{13}C \approx -25‰$) and bedrock magnesite ($\delta^{13}C \approx -4.0‰$), the groundwater DIC ($\delta^{13}C \approx -6.4‰$) only contains ~12% modern carbon from soil CO_2 (Fritz et al., 1978; Landmeyer and Stone, 1995). This value closely corresponds to the radiometric carbon datum of 11.3% modern carbon. It should be noted that dissolution of bedrock magnesite does not equate to a loss of CO_2 to the atmosphere, but rather a transformation from a bedrock source to a sedimentary basin. Bicarbonate from bedrock magnesite remains in solution along with modern bicarbonate and is ultimately precipitated in a new mineral form.

The $\delta^{13}C$ value of the wetland water (southeastern playa) DIC has an average carbon isotope value of 3.38‰ (two analyses). This is a ^{13}C-enrichment of +9.82‰ relative to the groundwater sampled from the nearby well (avg. $\delta^{13}C = -6.44‰$). This likely reflects the degassing of ^{13}C-depleted CO_2 and partly the preferential uptake of ^{12}C by cyanobacteria during photosynthesis (Fairchild et al., 2006; Pentecost and Spiro, 1990).

Isotopic compositions ($\delta^{18}O$ vs. $\delta^{13}C$) of carbonate samples from the wetland, grassland, and mound core are shown in Fig. 9. The three key samples from the wetland environment include the anoxic aragonite sediments, benthic mat carbonate, and evaporative crusts of nesquehonite. Degassing of CO_2 may cause $CaCO_3$ to become supersaturated and contribute to the precipitation of aragonite ($\delta^{13}C$ avg. = 5.06‰ and $\delta^{18}O$ avg. = 13.79‰; two analyses) found below the benthic microbial mats. Relatively ^{13}C- and ^{18}O-enriched carbonate minerals from the mats and the nesquehonite-rich crusts can in part be attributed to progressive evaporation of wetland water and to carbon isotope fractionation between DIC and Mg-carbonates. Deines (2004) noted that magnesite has a greater tendency to concentrate ^{13}C than other carbonate minerals, including aragonite. Other magnesium carbonate minerals, including hydromagnesite, dypingite, and nesquehonite are also likely to have this tendency. The benthic mat carbonate, containing both magnesium and calcium carbonate minerals (dypingite and aragonite), appears to have intermediate isotope values (Fig. 9A). Photosynthesis by cyanobacteria in the microbial mats preferentially removes bicarbonate anions containing ^{12}C and this may contribute to the precipitation of ^{13}C-enriched carbonates ($\delta^{13}C$ avg. = 6.66‰ and $\delta^{18}O$ avg. = 17.13‰; two analyses) relative to the aragonite sediments below the mats. A similar fractionation effect was noted by Pentecost and Spiro (1990) who found that calcite associated with *Rivularia* sp. was ~2‰ enriched in ^{13}C compared to travertine that was precipitated abiotically by CO_2 degassing. Evaporation of wetland water forms films and crusts of nesquehonite at the surface of the water and on exposed surfaces ($\delta^{13}C$ avg. = 9.26‰ and $\delta^{18}O$ avg. = 22.36‰; four analyses). These are enriched in both ^{13}C and ^{18}O relative to benthic mat carbonate, indicating that evaporative enrichment of ^{18}O and mineralogically-dependent fractionation of C is occurring.

As the wetland fills with carbonate sediments or as water levels decline, the sediments are exposed and evaporation becomes the dominate control on carbonate formation. Fig. 9B shows the isotopic compositions of the carbonates along the grassland transect, which represents an emerged wetland. These have been divided into two groups: (1) those collected above the water table and (2) those collected below. Samples collected at either end of the transect (near the wetland or the hydromagnesite mound ATC1) are further subdivided in Fig. 9B. The isotopic compositions of the near-wetland

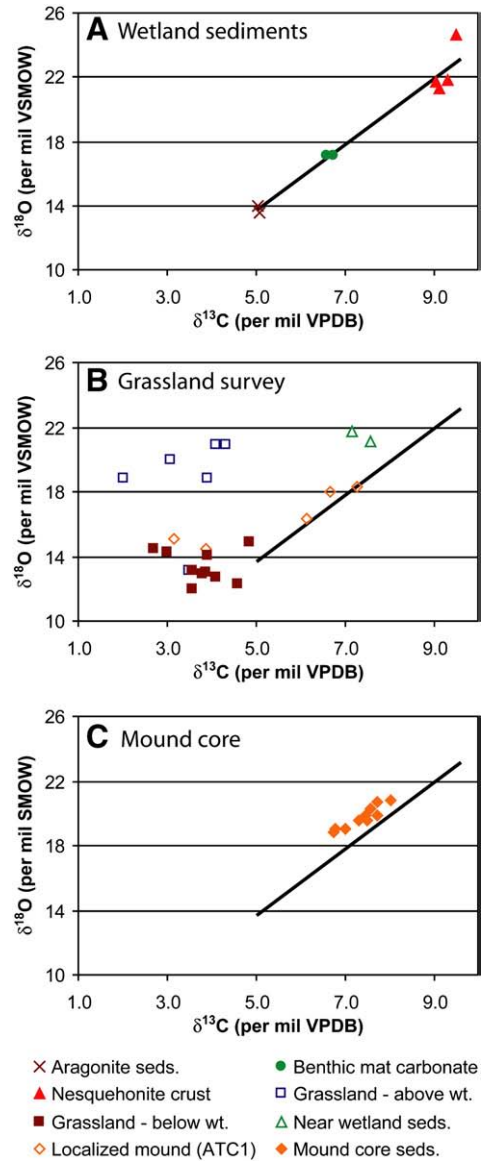

Fig. 9. Isotope compositions ($\delta^{18}O$ vs. $\delta^{13}C$) of sediment samples divided between three terrains (wetland sediments, grassland survey, and mound core) of the southeastern playa. A trend line for carbonates of the wetland is shown on all three graphs for comparison.

sediments ($\delta^{13}C$ avg. = 7.38‰ and $\delta^{18}O$ avg. = 21.42‰) have $\delta^{18}O$ values similar to those of the nesquehonite crusts and intermediate $\delta^{13}C$ values between those of the nesquehonite crusts and the benthic mat carbonate. The mineralogy (dypingite and nesquehonite), isotope values, and spatial distribution of these samples suggest an initial phase of biologically-aided precipitation followed by precipitation of carbonate minerals by evaporation.

Along the grassland transect, the samples from below the water table contain predominately ankerite and aragonite ($\delta^{13}C$ avg. = 3.49‰ and $\delta^{18}O$ avg. = 18.75‰), whereas those above the water table are mainly hydromagnesite ($\delta^{13}C$ avg. = 3.80‰ and $\delta^{18}O$ avg. = 13.36‰). The enriched $\delta^{18}O$ values of the above water table sediments are symptomatic of evaporative conditions near the surface. The similarity of $\delta^{13}C$ values between carbonate minerals above and below the water table indicates a common source of carbon, which is caused by an upward movement of water (with DIC) by capillary rise and possibly seasonal changes in the water table. The grassland sediments have lower $\delta^{13}C$ values relative to the wetland and mound sediments. Water collected at depth along the grassland

transect line, at 18.5 m from the wetland, had a $\delta^{13}C$ value of −1.10‰ for the DIC, which is between that of the well water (−6.44‰) and wetland water (3.38‰) DIC. In addition, the grass in the southeastern playa has a $\delta^{13}C$ of −27.3‰ (C_3 vegetation). Oxidation of the organic matter that is derived from the grassland vegetation contributes ^{13}C-depleted carbon, which is eventually respired as CO_2 by roots and soil biota. Some of this CO_2 escapes to the atmosphere while some is potentially precipitated as carbonate minerals (i.e., pedogenic carbonate), which may in part explain why the grassland sediments have depleted $\delta^{13}C$ values relative to the non-vegetated mounds.

Carbon and oxygen isotope data for the amalgamated mound carbonates (Fig. 9C) show decreasing trends that correspond to increasing depth. Carbon isotope values range from 8.0‰ (near surface) to 6.7‰ (VPDB) (at ~70 cm) and $\delta^{18}O$ values range from 20.8‰ to 18.8‰ (VSMOW). The relatively depleted isotopic values of deeper sediments compared to near surface deposits may be result of overprinting by the precipitation of carbonate minerals from depleted groundwater at depth and enrichment of ^{18}O by evaporation of near surface sediments.

5. Implications for CO_2 sequestration

In this study, we have examined the carbonation of magnesium silicates on a watershed scale and have emphasized the biological processes involved in the transformation of ultramafic rock to magnesium carbonate minerals in the context of a CO_2 sequestration model. The weathering of bedrock through purely abiotic processes is inherently slow under near-surface environmental conditions. In contrast, biologically-aided silicate dissolution that occurs in soils can be many orders of magnitude greater than weathering processes on bare rock surfaces.

Field observations, and mineralogical and isotope compositional analyses of carbonate minerals in the playas show three distinct depositional environments. Firstly, biological processes (including alkalization by cyanobacteria, sulphate reduction by SRB, and silica removal by diatoms) in the wetland create geochemical conditions for precipitation of carbonate minerals from evapoconcentrated waters. Eventually, sections of the wetland fill with carbonate sediments and convert to grassland, where precipitation of carbonate minerals by evapotranspiration is dominant. Although the second environment is limited, the physiology of the isolated sections of wetland is unique and leads to the formation of consolidated aragonite that includes pisolites. Thirdly, the hydromagnesite mounds developing from the capillary rise of Mg-rich groundwater, highlight the importance of a closed basin where evaporation can concentrate dissolved cations. The hydromagnesite deposits near Atlin overlie Holocene glacial till, demonstrating that these natural carbon sinks are stable over thousands of years (Grant, 1987). Therefore, artificial carbon sinks, created to mimic the conditions at Atlin, would be stable for the period of time needed to benefit society.

Lackner's (2002) study of mineral based sequestration of carbon considers the concept of stimulating the precipitation of carbonate minerals within specifically designed ponds or basins with excess alkalinity. He discusses the possibility of using biological processes that aid in the dissolution of alkaline rock (e.g., serpentine) and the precipitation of carbonate minerals. The biological processes described in this study, in conjunction with physical and chemical processes, could be applied for the purpose of CO_2 sequestration by artificially creating conditions similar to those at the Atlin site. In contrast to intensive, industrial processes previously proposed for CO_2 sequestration, the biological processes advocated here occur at near-surface conditions and do not require a substantial energy input. One potential application would be at mine facilities that contain large quantities of ultramafic tailings. Wilson et al. (2006) documented and quantified CO_2 bound in the form of magnesium carbonate minerals in chrysotile tailings from abandoned asbestos mines near Clinton Creek, Yukon Territory and Cassiar, British Columbia, Canada. Accelerated carbonation was attributed to the dramatic increase in surface area, caused by grinding and pulverizing of the ore during the mining process, which promoted chemical weathering. Carbon dioxide sequestration could be enhanced by restoring natural vegetation (i.e., a soil weathering horizon) on the tailings and by creating a specifically designed pond, similar to the southeastern playa–wetland, for leachate collection. These measures would both accelerate the dissolution of the tailings and provide a closed basin for evaporation and an appropriate habitat for microbes that aid in carbonate precipitation.

Acknowledgments

Research was funded by a Natural Sciences and Engineering Research Council of Canada (NSERC) Collaborative Research and Development Grant to G.M. Dipple and G. Southam. Support was also provided in part by an NSERC Accelerator Grant to G. Southam and an NSERC Post-Graduate Scholarship to I.M. Power. S. Wilson was funded by a Foundation Scholarship from the Mineralogical Association of Canada and an NSERC Canada Graduate Scholarship. Funding for fieldwork was partially provided by the Northern Scientific Training Program from Indian and Northern Affairs Canada and by a travel grant from the Mineralogical Association of Canada. We thank Dr. Elizabeth Webb for her helpful discussion on stable isotopes. We are grateful to Lyle Hansen, Eleanor Alesi, Noah Southam, and Joanne Woodhouse for their assistance in the laboratory and the field. Thanks to Norm Graham of Discovery Helicopters Ltd. and Fionnuala Devine for providing access to the southeastern playa and for their hospitality. Lastly, we thank the two reviewers for their helpful comments and suggestions.

References

Andrews, J.A., Schlesinger, W.H., 2001. Soil CO_2 dynamics, acidification, and chemical weathering in a temperate forest with experimental CO_2 enrichment. Global Biogeochemical Cycles 15 (1), 149–162.

Ash, C.H., Arksey, R.L., 1990. Tectonic setting of listwanite–lode gold deposits in the Atlin area. N.W. B.C., NTS (104N/12). Ministry of Energy, Mines and Petroleum Resources, Province of British Columbia. 1 pp.

Baker, P.A., Kastner, M., 1981. Constraints on the formation of sedimentary dolomite. Science 213 (4504), 214–216.

Benzerara, K., Menguy, N., Guyot, F., Vanni, C., Gillet, P., 2005. TEM study of a silicate–carbonate–microbe interface prepared by focused ion bean milling. Geochimica et Cosmochimica Acta 69 (6), 1413–1422.

Beukens, R.P., Gurfinkel, D.M., Lee, H.W., 1986. Progress at the isotrace radiocarbon facility. Radiocarbon 28 (2A), 229–236.

Boutton, T.W., 1991. Stable carbon isotope ratios of natural materials: II. Atmospheric, terrestrial, marine, and freshwater environments. In: Coleman, D.C., Fry, B. (Eds.), Carbon Isotope Techniques. Academic Press, Inc., San Diego, CA, USA, pp. 173–186.

Bowling, D.R., Pataki, D.E., Randerson, J.T., 2008. Carbon isotopes in terrestrial ecosystem pools and CO_2 fluxes. New Phytologist 178 (1), 24–40.

Braithwaite, C.J.R., Zedef, V., 1994. Living hydromagnesite stromatolites from Turkey. Sedimentary Geology 92 (1–2), 1–5.

Braithwaite, C.J.R., Zedef, V., 1996. Hydromagnesite stromatolites and sediments in an alkaline lake, Salda Gölü, Turkey. Journal of Sedimentary Research 66 (5), 991–1002.

British Columbia Ministry of Forests and Range: Biogeoclimatic Ecosystem Classification Program, 2008.

Bruker AXS, 2004, EVA V. 10.0: Release 2004 — User's Manual, Karlsruhe, Germany.

Burford, E.P., Fomina, M., Gadd, G.M., 2003. Fungal involvement in bioweathering and biotransformation of rocks and minerals. Mineralogical Magazine 67 (6), 1127–1155.

Das Sharma, S., Patil, D.J., Gopalan, K., 2002. Temperature dependence of oxygen isotope fractionation of CO_2 from magnesite–phosphoric acid reaction. Geochimica et Cosmochimica Acta 66 (4), 589–593.

Deines, P., 2004. Carbon isotope effects in carbonate systems. Geochimica et Cosmochimica Acta 68 (12), 2659–2679.

Environment Canada: National Climate Archive. Accessed on 2008.

Fairchild, I.J., Smith, C.L., Baker, A., Fuller, L., Spötl, C., Mattey, D., McDermott, F., E.I.M.F., 2006. Modification and preservation of environmental signals in speleothems. Earth-Science Reviews 75 (1–4), 105–153.

Ferris, F.G., Wiese, R.G., Fyfe, W.S., 1994. Precipitation of carbonate minerals by microorganisms: implications of silicate weathering and the global carbon dioxide budget. Geomicrobiology Journal 12 (1), 1–13.

Flanagan, L.B., Brooks, J.R., Varney, G.T., Berry, S.C., Ehleringer, J.R., 1996. Carbon isotope discrimination during photosynthesis and the isotope ratio of respired CO_2 in boreal forest ecosystems. Global Biogeochemical Cycles 10 (4), 629–640.

Fritz, P., Reardon, E., Barker, J., Brown, R., Cherry, J., Killey, R., McNaughton, D., 1978. Carbon isotope geochemistry of a small groundwater system in northeastern Ontario. Water Resources Research 14 (6), 1059–1067.

Gerdemann, S.J., O'Connor, W.K., Dahlin, D.C., Penner, L.R., Rush, H., 2007. Ex situ aqueous mineral carbonation. Environmental Science and Technology 41, 2587–2593.

Giammar, D.E., Bruant, R.G., Peters, C.A., 2005. Forsterite dissolution and magnesite precipitation at conditions relevant for deep saline aquifer storage and sequestration of carbon dioxide. Chemical Geology 217 (3–4), 257–276.

Grant, B., 1987. Magnesite, brucite and hydromagnesite occurrences in British Columbia. Open File Report of the British Columbia Geological Survey Branch No 1987-13.

Hansen, L.D., 2005. Geologic setting of listwanite, Atlin, B.C.: Implications for Carbon Dioxide Sequestration and Lode-Gold Mineralization. The University of British Columbia, Vancouver.

Hansen, L.D., Dipple, G.M., Gordon, T.M., Kellett, D.A., 2005. Carbonated serpentinite (listwanite) at Atlin, British Columbia: a geological analogue to carbon dioxide sequestration. Canadian Mineralogist 43, 225–239.

Haynes, R.H. (Ed.), 1998. The Canadian System of Soil Classification. Agriculture and Agri-Food Canada. 187 pp.

Hillgärtner, H., Dupraz, C., Hug, W., 2001. Microbially induced cementation of carbonate sands: are micritic meniscus cements good indicators of vadose diagenesis? Sedimentology 48, 117–131.

Holland, H.D., Lazar, B., McCaffrey, M., 1986. Evolution of the atmosphere and oceans. Nature 320 (6057), 27–33.

Kastner, M., 1984. Control of dolomite formation. Nature 311 (5985), 410–411.

Kelemen, P.B., Matter, J., 2008. In situ carbonation of peridotite for CO_2 storage. Proceedings of the National Academy of Sciences 105 (45), 17295–17300.

Lackner, K.S., 2002. Carbonate chemistry for sequestering fossil carbon. Annual Review of Energy and the Environment 27, 193–232.

Lackner, K.S., Wendt, C.H., Butt, D.P., Joyce, E.L., Sharp, D.H., 1995. Carbon dioxide disposal in carbonate minerals. Energy 20 (11), 1153–1170.

Lahav, O., Morgan, B.E., Loewenthal, R.E., 2001. Measurement of pH, alkalinity and acidity in ultra-soft waters. Water SA 27 (4), 423–431.

Landmeyer, J.E., Stone, P.A., 1995. Radiocarbon and δ13C values related to ground-water recharge and mixing. Ground Water 33 (2), 227–234.

McLean, R.J.C., Jamieson, H.E., Cullimore, D.R., 1997. Formation of nesquehonite and other minerals as a consequence of biofilm dehydration. World Journal of Microbiology & Biotechnology 13 (1), 25–28.

Metz, B., Davidson, O., de Coninck, H.C., Loos, M., Meyer, L.A., 2005. IPCC, 2005: IPCC special report on carbon dioxide capture and storage. Prepared by Working Group III of the Intergovernmental Panel on Climate Change. Cambridge University Press, Cambridge, United Kingdom. 442 pp.

Mora, G., Raich, J.W., 2007. Carbon-isotopic composition of soil-respired carbon dioxide in static closed chambers at equilibrium. Rapid Communications in Mass Spectrometry 21 (12), 1866–1870.

Obst, M., Dittrich, M., Kuehn, H., 2006. Calcium adsorption and changes of the surface microtopography of cyanobacteria studied by AFM, CFM, and TEM with respect to biogenic calcite nucleation. Geochemistry Geophysics Geosystems 7 (6).

Oh, N., Richter, D.D.J., 2004. Soil acidification induced by elevated atmospheric CO_2. Global Change Biology 10 (11), 1936–1946.

Parkhurst, D.L., Appelo, C.A.J., 1999. User's guide to PHREEQC (version 2) A computer program for speciation, batch reaction, one-dimensional transport, and inverse geochemical calculations. U.S., Geological Survey Water-Resources Investigations Report 99-4259. 312 pp.

Pentecost, A., 1995. Significance of the biomineralizing microniche in a Lyngbya (cyanobacterium) travertine. Geomicrobiology Journal 13 (4), 213–222.

Pentecost, A., Spiro, B., 1990. Stable carbon and oxygen isotope composition of calcites associated with modern freshwater cyanobacteria and algae. Geomicrobiology Journal 8 (1), 17–26.

Power, I.M., Wilson, S., Thom, J.M., Dipple, G.M., Southam, G., 2007. Biologically induced mineralization of dypingite by cyanobacteria from an alkaline wetland near Atlin, British Columbia, Canada. Geochemical Transactions 8, 13.

Renaut, R.W., 1990. Recent carbonate sedimentation and brine evolution in the saline lake basins of the Cariboo Plateau, British Columbia, Canada. Hydrobiologia 197, 67–81.

Renaut, R.W., 1993. Morphology, distribution, and preservation potential of microbial mats in the hydromagnesite–magnesite playas of the Cariboo Plateau, British-Columbia, Canada. Hydrobiologia 267 (1–3), 75–98.

Riding, R., 2000. Microbial carbonates: The geological record of calcified bacterial–algal mats and biofilms. Sedimentology 47 (Suppl. 1), 179–214.

Riding, R., 2006. Cyanobacterial calcification, carbon dioxide concentrating mechanisms, and Proterozoic–Cambrian changes in atmospheric composition. Geobiology 4, 299–316.

Roberts, J.A., Bennett, P.C., Gonzalez, L.A., Macpherson, G.L., Milliken, K.L., 2004. Microbial precipitation of dolomite in methanogenic groundwater. Geology 32 (4), 277–280.

Russell, M.J., Ingham, J.K., Zedef, V., Maktav, D., Sunar, F., Hall, A.J., Fallick, A.E., 1999. Search for signs of ancient life on Mars: expectations from hydromagnesite microbialites, Salda Lake, Turkey. Journal of the Geological Society, London 156, 869–888.

Schultze-Lam, S., Fortin, D., Davis, B.S., Beveridge, T.J., 1996. Mineralization of bacterial surfaces. Chemical Geology 132 (1–4), 171–181.

Schwartzman, D.W., Volk, T., 1989. Biotic enhancement of weathering and the habitability of Earth. Nature 340 (6233), 457–460.

Siefritz, W., 1990. CO_2 disposal by means of silicates. Nature 345, 486.

Solomon, S., Qin, D., Manning, M., Chen, Z., Marquis, M., Averyt, K.B., Tignor, M., Miller, H.L. (Eds.), 2007. IPCC, 2007: Climate Change 2007: The Physical Science Basis. Contribution of Working Group I to the Fourth Assessment Report of the Intergovernmental Panel on Climate Change. Cambridge University Press, Cambridge, United Kingdom. 996 pp.

Stamatakis, M.G., Renaut, R.W., Kostakis, K., Tsivilis, S., Stamatakis, G., Kakali, G., 2007. The hydromagnesite deposits of the Atlin area, British Columbia, Canada, and their industrial potential as fire retardant. Proceedings of the 11th International Congress. Bulletin of the Geological Society of Greece, p. 10.

Starr, M., Lindroos, A.J., 2006. Changes in the rate of release of Ca and Mg and normative mineralogy due to weathering along a 5300-year chronosequence of boreal forest soils. Geoderma 133 (3–4), 269–280.

Thompson, J.B., Ferris, F.G., 1990. Cyanobacterial precipitation of gypsum, calcite, and magnesite from natural alkaline lake water. Geology 18 (10), 995–998.

Ullman, W.J., Kirchman, D.L., Welch, S.A., Vandevivere, P., 1996. Laboratory evidence for microbially mediated silicate mineral dissolution in nature. Chemical Geology 132, 11–17.

van Lith, Y., Warthmann, R., Vasconcelos, C., McKenzie, J.A., 2003a. Microbial fossilization in carbonate sediments: a result of the bacterial surface involvement in dolomite precipitation. Sedimentology 50 (2), 237–245.

van Lith, Y., Warthmann, R., Vasconcelos, C., McKenzie, J.A., 2003b. Sulphate-reducing bacteria induce low-temperature Ca-dolomite and high Mg-calcite formation. Geobiology 1, 71–79.

Verardo, D.J., Froelich, P.N., McIntyre, A., 1990. Determination of organic carbon and nitrogen in marine sediments using the Carlo Erba NA-1500 Analyzer. Deep-Sea Research 37 (1), 157–165.

Webb, E.A., Schwarcz, H.P., Healy, P.F., 2004. Detection of ancient maize in lowland Maya soils using stable carbon isotopes: evidence from Caracol, Belize. Journal of Archaeological Science 31 (8), 1039–1052.

Wilson, S., Raudsepp, M., Dipple, G.M., 2006. Verifying and quantifying carbon fixation in minerals from serpentine-rich mine tailings using the Rietveld method with X-ray powder diffraction data. American Mineralogist 91 (8–9), 1331–1341.

Xu, T., Apps, J.A., Pruess, K., 2005. Mineral sequestration of carbon dioxide in a sandstone–shale system. Chemical Geology 217, 295–318.

Young, G.A., 1916. Hydromagnesite deposits of Atlin. B.C. Geological Survey of Canada Summary Report, pp. 50–61.

Zaitseva, L.V., Orleanskii, V.K., Alekseev, A.O., Ushatinskaya, G.T., Gerasimenko, L.M., 2007. Transformation of carbonate minerals in a cyano-bacterial mat in the course of laboratory modeling. Microbiology 76 (3), 342–356.